IEEE Robotics and Automation Letters (RA-L) paper, presented at ICRA 2026, Vienna, Austria. Cite as RA-L paper.

Design of a Variable Stiffness Quasi-Direct Drive Cable-Actuated Tensegrity Robot

Jonathan Mi[1], Wenzhe Tong[1], Yilin Ma[1] and Xiaonan Huang[1]

***Abstract*—Tensegrity robots excel in tasks requiring extreme levels of deformability and robustness. However, there are challenges in state estimation and payload versatility due to their high number of degrees of freedom and unconventional shape. This paper introduces a modular three-bar tensegrity robot featuring a customizable payload design. Our tensegrity robot employs a novel Quasi-Direct Drive (QDD) cable actuator with low-stretch polymer cables to achieve accurate proprioception without needing external force or torque sensors. The design allows for on-the-fly stiffness tuning for better environment and payload adaptability. In this paper, we present the robot's design, fabrication, assembly, and experimental results. Experimental data demonstrates the high accuracy cable length estimation (<1% error relative to bar length) and variable stiffness control of the cable actuator up to 7 times the minimum stiffness for self support. The shape morphing and stiffness tuning capabilities are leveraged in two realistic demonstrations. The presented tensegrity robot is a platform for future advancements in autonomous operation and open-source module design. Open source design files are available at https://github.com/UMich-HDRLab/tensegrity-robot-hardware/.**

***Index Terms*—Soft Robot Materials and Design, Compliant Joints and Mechanisms, Flexible Robotics**

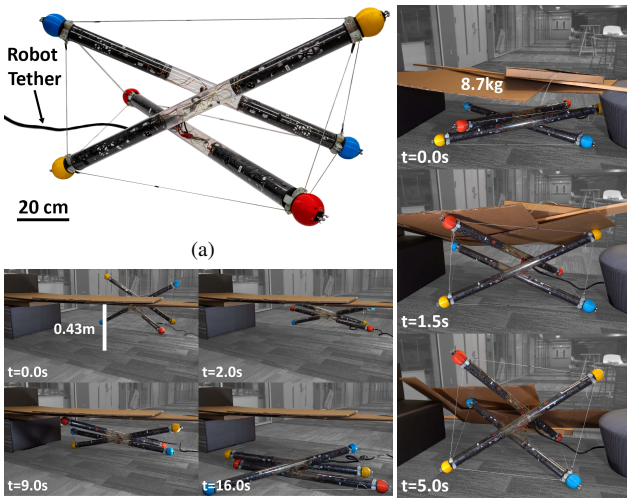

Fig. 1. The (a) assembled three-bar tensegrity robot. The tether attaches to the middle of each bar through the triangular face of the structure. The robot uses (b) a compact gait to crawl under a 0.43 m tall space and (c) a high stiffness modality to lift 8.7 kg of collapsed debris.

I. Introduction

TENSEGRITY, or tensional integrity structures, represent a unique class of architectural forms comprising rigid elements, such as bars or struts, and tensile components, such as cables or tendons. These structures exhibit exceptional strength-to-weight ratios, as the bar elements are subjected exclusively to axial compressive forces, while the cables experience only tensile forces [1]. By introducing actuation, sensor feedback, spatial perception, and autonomy, tensegrity structures are transformed into tensegrity robots with inherent robustness to dropping and load bearing, added locomotion, flexibility, and compactness. These robots are highly deformable, which allows for impact resistance and the ability to collapse into smaller volumes. This deformability enables efficient storage and facilitates navigation through constrained passageways, over obstacles, and even up steep inclines [2].

Autonomous robots equipped with motion planning, feedback control, and computer vision systems heavily depend on precise state estimation, including position, orientation, and velocity [3]. The high number of degrees of freedom (DoF) and complex dynamics presents significant challenges in advancing tensegrity robots to full autonomy. Current tensegrity robots are limited by state estimation inaccuracies, which can be several percent of the robot's bar length [4]. Percent of bar length (PBL) is utilized as the error metric since the bar length is a representative measure of the overall size of a tensegrity robot. One specific limitation in state estimation is cable length estimation. Since the distance between all the bars is constrained by the cables, inaccurate cable length estimation directly leads to poor state reconstruction. Without accurate state data, rolling locomotion could also be compromised as most tensegrity robots rely on shifting their center of mass (COM) via shape morphing. Integrating computer vision systems is further challenged by the space requirements of a powerful computing unit. Tensegrity robots typically have very little usable internal volume within their structure. The bars also need to be skinny relative to the robot's overall size to avoid rod collisions, which could lead to radial impact forces and subsequent structural failure. The result is a tight integration space that complicates the incorporation of onboard computing.

Moreover, current tensegrity robots face variable stiffness limitations, where variable stiffness refers to the ability to modulate the resistance to deformation in response to applied forces, due to the strict coupling of stiffness and shape.

Manuscript received: February, 6, 2025; Revised April, 27, 2025; Accepted June, 8, 2025.

This paper was recommended for publication by Editor Yong-Lae Park upon evaluation of the Associate Editor and Reviewers' comments. This work was supported by the National Science Foundation under the Graduate Research Fellowship No. DGE 2241144 and the startup fund from the Robotics Department at the University of Michigan.

[1]The authors are with the Robotics Department, University of Michigan-Ann Arbor, Ann Arbor, MI, USA {jjomi, wenzhet, yilinma, xiaonanh}@umich.edu

Digital Object Identifier (DOI): see top of this page.

IEEE Robotics and Automation Letters (RA-L) paper, presented at ICRA 2026, Vienna, Austria. Cite as RA-L paper.

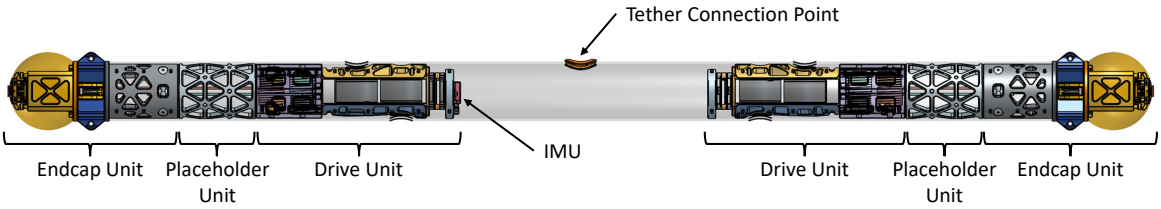

Fig. 2. Internal view of a single tensegrity robot bar. Each bar contains two endcaps and two drive units. The inertial measurement unit (IMU) is mounted on the bottom of one of the drive units and has its z-axis aligned with the central axis of the bar. The placeholder unit inserted between the endcap and the drive unit demonstrates a feasible location for an additional module. Additional modules can also be inserted in the space between the two drive units.

Decoupling these two factors could enable new functionalities, particularly in unstructured terrain, by allowing robots to adjust rigidity and maintain shape under varying loads. However, current cable driven actuator designs can only achieve variable stiffness via cable pretension [5], [6], which cannot be adjusted once the robot is in operation.

The tensegrity robot proposed in this paper, shown in Fig. 1a, makes several key contributions towards achieving full autonomy. First, it achieves accurate proprioception through the novel implementation of Quasi-Direct Drive (QDD) cable actuators. The design eliminates the need for force sensors, torque sensors, or series elastic elements, thereby simplifying the system and reducing weight. Second, the QDD cable actuators facilitate variable stiffness control, allowing for on-the-fly stiffness tuning and precise control of cable length and force. Third, the modular exoskeleton design facilitates varying bar and cable actuator counts for different configurations and effectively addresses bar space constraints by providing a robust and flexible platform for integrating advanced sensing and on-board computing systems. Finally, by leveraging shape morphing and stiffness tuning, we demonstrate (1) load carrying capacity for locomotion, (2) navigation through height constrained areas, and (3) lifting collapsed debris. These advancements collectively contribute to the development of autonomous tensegrity robots.

The remainder of this paper is organized as follows: Section II provides a review of related works. Sections III, IV, and V detail the mechanical, electrical, and software design of the robot, respectively. Section VI presents the results from cable actuator and robot testing. Finally, Section VII summarizes the contributions of the paper and outlines the directions for future work.

II. Related Works

Due to the unconventional structure of tensegrity robots, a diverse range of different actuation strategies have been explored. Series elastic actuators (SEAs) [7] are widely used for cable actuation to provide structural compliance. Various approaches have been employed, including cable-spring assemblies [8]–[10] and compliant cables [11], [12]. However, these methods pose challenges for state estimation due to the difficulty of accurately measuring the length of elastic elements. Moreover, cable-spring assemblies either require an external spring, which can become tangled [8], or a large internal spring, which occupies a significant amount of space within the bar. Elastomer-based tendons with capacitance-based sensing [13] offer accurate elastic length estimation when combined with cable actuators. However, they are challenging to manufacture and difficult to scale for larger robots. Additionally, they are susceptible to drift, creep under constant stress, and damage from sharp objects or obstacles.

Several works have achieved shape changing by using pneumatic or linear actuators in place of cables-spring assemblies [14]–[16]. However, linear actuators are not ideal replacements due to their susceptibility to damage from shock loads. Besides, this method of locomotion generally results in slower speeds compared to other techniques. For example, the TT2 robot proposed by Kim *et al.* achieved a maximum speed of only 0.014 body lengths per second (BLPS), or 0.01 m/s [15]. Pneumatic skins [17] have proven effective but, like elastomer-based tendons, are difficult to scale up and require large off-board compressors.

Vibration actuators offer a promising alternative for fast and low-complexity locomotion compared to traditional cable actuators [18]. Rieffel *et al.* demonstrated speeds of up to 0.88 BLPS (0.115 m/s). However, intense vibrations are problematic for computer vision systems, which struggle with high-frequency perturbations [19]. Furthermore, vibration-based locomotion cannot handle obstacle traversal. Consequently, this approach is incompatible with the goals of developing autonomous and intelligent tensegrity robots.

While not yet utilized in tensegrity robots, electromechanical variable stiffness actuators (EMAVSAs) have been used to achieve variable stiffness control in joints [20]. However, these actuators are often limited in rotational range and require additional actuators, and therefore space, to achieve variable stiffness functionality. This makes them unsuitable for tensegrity cable spool actuation.

Our work advances the cable and spool actuated architecture by introducing QDD actuators, which are well-established in modern legged and humanoid robots. QDD actuators are defined by their use of high torque motors with very low gear ratios, which allows them to deliver high torque output while remaining easily backdrivable. This reduces the complexity, efficiency losses, and backlash typically associated with higher gear ratios. QDD actuators are favored in these fields because they can control joint stiffness and detect external forces through motor current sensing, alleviating the need for external torque sensors, force sensors, or series elastic elements [21].

III. Mechanical Design

While the tensegrity robot depicted in Fig. 1a features a three-bar configuration, the minimum number of bars required to form a class 1 tensegrity structure capable of locomotion [22], this design is not limited to just three bars. Each

IEEE Robotics and Automation Letters (RA-L) paper, presented at ICRA 2026, Vienna, Austria. Cite as RA-L paper.

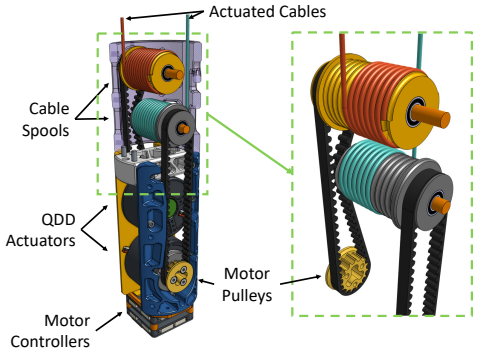

Fig. 3. Cutaway view of the drive unit CAD model. The red and teal strings are the actuated cables. The right side of the image shows a close up of the belt driven, dead-axle, grooved cable spool design. The motor controllers are located at the base of the unit.

tensegrity bar is a standalone unit, allowing the system to be easily extended to configurations with four, five, six, or more bars. When collapsed, the robot can fit into a 1.45 m long, 0.21 m diameter cylinder. When fully expanded, it can reach a maximum height of 1.0 m.

The bar exoskeleton is constructed from a polycarbonate tube with a length of 1.2 m, a diameter of 76 mm, and a wall thickness of 3 mm. Polycarbonate is selected for its excellent impact resistance and ease of fabrication. The tube exoskeleton provides a modular framework for optimized sensor and camera placement, enabling enhanced perception and adaptable robotic functionalities.

Currently, two fundamental modules have been developed: the drive unit and the endcap unit, both required for basic robot locomotion. An assembled bar, as illustrated in Fig. 2, incorporates two of each of these units. With each bar weighing 4.0 kg, the total weight of the three-bar robot is 12.0 kg. The mechanical design of the robot is detailed in the following.

A. Drive Unit

The drive unit houses the powertrain responsible for actuating the cables of the robot. Each tube accommodates two such units, enabling a maximum of up to four actuated cables per bar. To achieve variable cable length, tension, and operation mode while maintaining precise cable length sensing, QDD actuators are employed. QDD actuators are required for high-speed force control [23] of the cables. They enable the robot to replicate the operation of an SEA without the cable length inaccuracies associated with SEAs when using purely encoder-based cable length feedback. The design, illustrated in Fig. 3, does not require additional force or torque sensors.

1) Actuator Design: The expected cable forces are modeled to determine the actuator torque requirements. Modeling of Tensegrity Structure (MOTES) simulation software [24] is utilized to estimate the expected cable forces during locomotion. A video of the simulation can be found in SI Video S6. Each bar is assigned a weight and we assume the cables are lightweight with negligible mass.

With an estimated bar mass of 5 kg, the maximum force simulated in the cables for locomotion is 289 N with an average force of 97 N. The 5 kg estimate includes a large 1 kg allowance for future untethered components including the computing unit and battery. The torque on the motor can be related to the force on the cable with:

$$F_c = \frac{\tau_m}{r_s} \tag{1}$$

where r_s is the radius of the spool and τ_m is the torque on the output of the motor gearbox. The cable spool has a radius of 0.015 m, meaning the actuator must be able to provide a maximum torque of 4.33 Nm and an average torque of 1.45 Nm for locomotion.

The chosen actuator is the GIM4310 brushless direct current (BLDC) motor, which has an integrated 10:1 planetary reduction gearbox. It provides a continuous torque of 3 Nm and a stall torque of 6 Nm, which meets the simulated torque requirement with some margin. The single-stage planetary gear reduction is the only reduction in the system, contributing to a relatively transparent transmission—an important consideration in the design of QDD actuators.

2) Cable Spool: Custom 30-mm diameter grooved spools with integrated pulleys shown in Fig. 3 are used to actuate the cables. The grooved spool allows for more controlled winding compared to a bare spool, which improves cable length measurement accuracy [25]. Each spool can wind and unwind 1.2 m of cable. The integrated pulley and dead-axle design of the spool removes backlash that would otherwise be present in a live-axle design. The end of the cable is held in place with a knot in the spool.

3) Cable Selection: Various cable materials have been employed in tensegrity robots and cable-driven parallel robots, both of which utilize cable spool actuators for motion and force transmission. Although steel cable has traditionally been used in cable-driven robots, modern polymers such as ultra-high-molecular-weight polyethylene (UHMWPE) have proven to be both stronger and lighter than steel cables of the same diameter and length [27]. For meter-scale robots, the choice of cable material is particularly critical, as compared to centimeter-scale systems, due to the significantly larger forces involved in locomotion and impacts. The strength, weight, and elongation of several cable options are presented in Table I. Cable elongation is given at 30% of the cable's maximum breaking load (MBL).

TABLE I
COMPARISON OF CABLE MATERIALS

Material	MBL (kN)	Weight (g/m)	Elongation (%)	Ref.
⌀2 mm Steel	2.75	15.2	< 2	[8]
⌀4 mm Nylon	3.4	9.02	13-15	[12]
⌀1.4 mm Vectran	2.2	6.8	< 1	[26]
⌀2 mm Dyneema	4.5	3.72	<0.7	This work

For the tensegrity robot presented in this work, HTS-75 12-strand Dyneema® SK-78 UHMWPE cord with a diameter of 2 mm is selected. The Dyneema cord offers a tensile strength of 4.5 kN and less than 0.7% elongation at 30% of its MBL. Compared to steel cable, the flexibility of the polymer cable allows for the use of smaller pulleys and cable spools. For optimal performance, steel cables require pulleys that are 25 times larger than the cable diameter [28], while polymer cables only need pulleys that are 10 times the

IEEE Robotics and Automation Letters (RA-L) paper, presented at ICRA 2026, Vienna, Austria. Cite as RA-L paper.

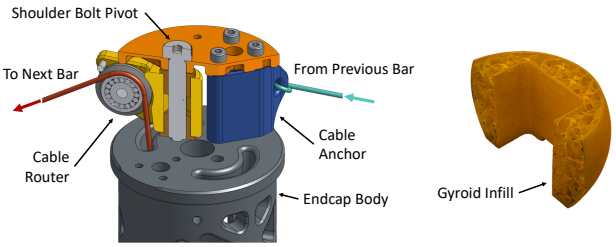

Fig. 4. A (a) Sectional view of the endcap cable router and cable anchor model. One of two cable routers is on the left in yellow and one of two cable anchors is on the right in blue. The sectional view shows the swiveling and cable guide mechanism of the cable router. The compliant cap is mounted on top of the orange plate. The (b) sliced open compliant cap reveals its internal structure. The low density gyroid infill allows for uniform compliance in all directions. The part is printed with 95A TPU filament.

cable diameter [29]. Therefore, without using polymer cable, it would have been impossible to package all the required components into the exoskeleton tube. Compared to the nylon cord used in SUPERballv2 [12], the elongation factor of the UHMWPE cord is significantly smaller, leading to better cable length estimation. Vectran is another excellent choice of polymer cable due to its low stretch properties, but it is difficult to acquire and cost-prohibitive.

B. Endcap Unit

The endcap unit is the contact point between the robot and the environment and is responsible for routing cables from the drive units to the anchor points on other bars. Ensuring smooth cable routing is important for minimizing cable friction to achieve more accurate cable length estimation.

1) Compliant Cap: The sphere on the endcap is 3D printed using 95A thermoplastic polyurethane (TPU) with a 7% gyroid infill pattern. The low infill percentage in combination with the gyroid pattern ensures the sphere is uniformly compliant in all directions. A sectional view of the printed cap is shown in Fig. 4b. The center of the cap has a rigid internal frame to support future sensor attachment, such as contact sensors, force sensors, or cameras.

2) Cable Router and Cable Anchor: The cable routing system consists of swiveling cable pulleys and anchors designed to facilitate the smooth transfer of cables between bars. Each cable router utilizes a 20 mm diameter cable pulley to redirect cables from the cable spool to the next adjacent bar. The router swivels horizontally on a shoulder bolt, with a wide 128-degree range that ensures smooth cable movement across all robot shape configurations. A stainless steel pin, positioned just above the pulley, prevents dislodging of the cable from the pulley groove.

The cable anchor serves dual purposes: it functions as the attachment point for the end of each actuated cable and acts as a spacer between the endcap body and the compliant cap mounting plate. A sectional view of the cable router and cable anchor is shown in Fig. 4a. Each endcap incorporates one pair of cable routers and one pair of cable anchors, arranged such that the routers and anchors are alternated and clocked 90 degrees apart from each other.

C. Manufacturing

The robot hardware is produced using metal machining, Fused Deposition Modeling (FDM), and Stereolithography Apparatus (SLA) 3D printing. Shafts and axles are machined from high-strength 7075-T6 aluminum. The drive and endcap unit bodies are printed with Polylactic Acid (PLA). High-strength parts, such as the motor pulley and motor mounts, are printed using carbon fiber reinforced Nylon 6 (PA6-CF) through FDM. Components facing stress in two directions, like cable router pulley brackets and cable anchors, are printed with Formlabs Durable resin using SLA for its isotropic properties, which are better suited for handling multi-directional stresses compared to the anisotropic properties of FDM-printed components.

IV. Electrical Design

The electrical system, illustrated in Fig. 5, includes a power supply, motor controllers, cable actuators, an inertial measurement unit (IMU) sensor, robot controller, host device, and cable harness. The following discusses the design of each component in detail.

A. Robot Power

The electronics are powered by a single 300 W bench power supply providing 24 V. Power is distributed through 18 AWG wires, with each bar receiving power from its own pair. These power wires are bundled with the signal wires within a sheathed wire harness, as illustrated in Fig. 1a.

B. Motor Controller

MJBots moteus-n1 BLDC motor controllers are chosen to control the cable actuators. These controllers are selected for their ability to meet motor power requirements, small form factor, and controller area network (CAN) bus connectivity. The BLDC motors are operated using field oriented control (FOC) to enhance efficiency and controllability. For torque feedback, low-side current sense resistors are used by the motor controller. The motor controllers were modified to use 10 mOhm current sense resistors instead of the stock 0.5 mOhm resistors to improve current sensing and therefore torque sensing capabilities.

For motor position feedback, an AS5047 absolute magnetic encoder connected to the motor controller through a 4-wire Serial Peripheral Interface (SPI) is utilized. The absolute position functionality is required for motor commutation. For cable length estimation, the encoder operates as a relative encoder and must be initialized to a home position when the robot is powered on. This initialization is achieved by manually setting each cable to the software specified initial length. The cable length l_c can then be estimated using:

$$l_c = 2\pi r_s n \tag{2}$$

where n is the number of encoder turns. While integrating a multi-turn absolute encoder directly on the spool would eliminate the need for manual initialization, this approach is currently constrained by the limited space available in the motor housing, posing significant design challenges.

IEEE Robotics and Automation Letters (RA-L) paper, presented at ICRA 2026, Vienna, Austria. Cite as RA-L paper.

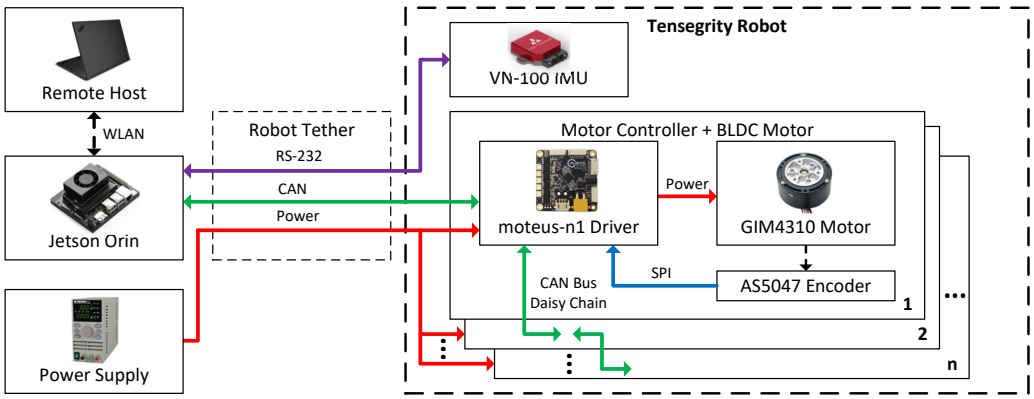

Fig. 5. Block diagram of the tensegrity robot electrical system. Robot power and control signals are wired through the robot tether. The controller area network (CAN) bus is daisy-chained from the Jetson Orin to each of the moteus motor controllers.

C. Additional Sensors

The integration of QDD actuators minimizes the number of sensors needed for proprioception. The sole additional sensor employed is a VectorNAV VN-100 inertial measurement unit (IMU), which communicates with the robot controller via RS-232. This communication cable is incorporated into the wire harness.

D. Robot Controller

The robot controller is a NVIDIA Jetson Orin, interfacing with the robot CAN bus via a Texas Instruments TCAN1042 CAN transceiver. Motor control signals are transmitted over the robot CAN bus, which is configured in a daisy-chain topology as shown in Fig. 5. This topology extends from the Orin through each motor controller and terminates after the last motor controller. The use of daisy-chain topology reduces wiring complexity, requiring only a single pair of CAN wires in the wire harness to connect all control signals to the robot controller. To control the robot, a remote host is connected to the robot controller via a wireless local area network (WLAN).

V. Software Design

The software stack to control the tensegrity robot consists of a high-level robot controller, cable actuator controllers, and low-level motor controllers. Fig. 6 illustrates the block diagram of the software stack. Currently, basic teleoperation allows the robot to roll forward, backward, turn, and change stiffness.

A. Cable Actuator Control

The QDD cable actuator enables dynamic cable control that can be adjusted in real-time to suit different situations. For instance, if the IMU detects that the robot is falling, the robot can be made softer to better absorb the shock load. Conversely, if the robot is carrying a payload, it can be made stiffer to hold shape. The following three cable actuator control modes have been developed:

1) **Length mode:** The cable is set to a specified cable length l_{sp} with proportional derivative (PD) control that enforces a minimum cable force to ensure that the cable is always under tension:

$$F_c = \begin{cases} k_p(l_c - l_{sp}) + k_d \frac{d(l_c - l_{sp})}{dt} + F_f & l_c \geq l_{sp} \\ F_f & l_c < l_{sp} \end{cases} \quad (3)$$

where k_p and k_d are the proportional and derivative gain values of the PD controller, and F_f is the manually tuned feed forward force to account for frictional losses.

2) **Spring mode:** The cable acts as a spring. The actuator will imitate the specified spring function:

$$F_c = f(l_c) \quad (4)$$

where $f(l_c)$ is any arbitrary function dependent on the current cable length.

3) **Constant force mode:** A constant force is applied to the cable, regardless of the current cable length.

Additional low level motor position and FOC current control loops on the motor controller microcontroller respond to the cable actuator controller outputs.

To achieve variable stiffness control, the control constants in both length mode and spring mode can be adjusted. In length mode, k_p and k_d function as the spring constant and damping coefficient, respectively, allowing the stiffness of the system to be varied by altering these gain values. In spring mode, any arbitrary function can be employed to define cable force. For instance, a linear spring can be represented by the following:

$$f(l_c) = k_s l_c \quad (5)$$

where k_s denotes the specified spring constant. Alternatively, a possible non-linear spring function can be represented as the following:

$$f(l_c) = k_1 l_c^{k_2} + k_3 \quad (6)$$

where k_1 is a scaling factor, k_2 is the exponential factor, and k_3 is the minimum cable force. These parameters can be dynamically adjusted to suit different operational scenarios.

B. Teleoperation

For teleoperation, the teleoperator uses the remote host to publish an encoded control message onto a Lightweight Communications and Marshalling (LCM) [30] network. This

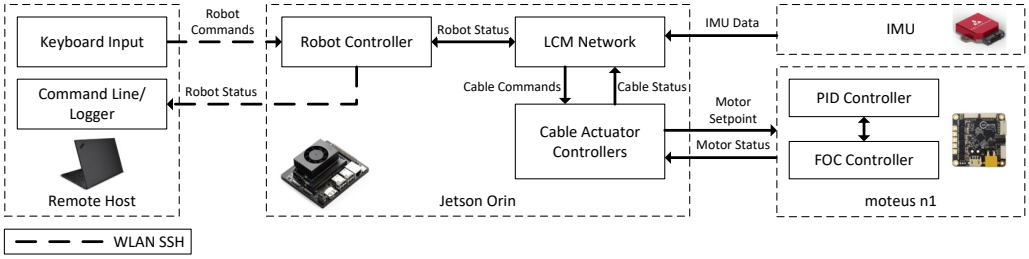

Fig. 6. Block diagram of the software stack. The remote host sends encoded control messages to the robot controller, which then communicates with the IMU and cable actuator controllers via the LCM network. The cable actuator controllers exchange motor setpoint and status data with the low-level motor position and FOC current controllers.

message includes the timestamp, cable control parameters, and the cable actuator ID. The cable control parameters specify the cable control mode and associated variables, such as cable length and tension. The robot controller decodes the LCM messages, computes the motor setpoints, and sends commands to the moteus motor controllers over the CAN bus to achieve the setpoints. The cable actuator controller sends a status messages back to the remote host for diagnosis and monitoring.

VI. Experimental Results

Experiments were conducted to verify the cable length estimation accuracy and variable stiffness control. The full robot was also tested to verify locomotion and variable stiffness functionality.

A. Cable Length Accuracy

Cable length estimation is critical for accurate state estimation. Errors in cable length estimation can arise from several sources, including cable stretch, cable wrap on the spool, and encoder resolution. The experiment was conducted using the setup shown in Fig. 7. This setup comprised a half-length bar, which included one drive unit and one endcap unit. The half-bar was attached to the base of a universal testing machine (Instron 68SC-5), with the cable guide's output aligned to the center of the machine's load cell. The actuated cable was attached to the load cell using a carabiner clip. To evaluate cable length estimation, the height of the load cell was adjusted from 0.05 m to 0.65 m in 0.05 m increments. The estimated cable lengths were recorded for loads of 50 N, 100 N, 150 N, and 200 N, which reflects the typical operational range of the cable actuator. Nylon paracord, used in Superballv2 [12], was also tested for comparison.

Results shown in Fig. 8 indicate that the cable length estimation error with the Dyneema cable was less than 1 PBL across the tested cable length and force range. On the other hand, the Nylon cable saw as much as 11 PBL error. The error also increased with force, which is the expected outcome of the more elastic cable as it will stretch more. Compared to some existing state estimation techniques, like external ranging sensors [31], external cameras [32], or robotic skins [33], the proposed approach to cable length estimation demonstrates significantly improved accuracy without the need for additional sensors.

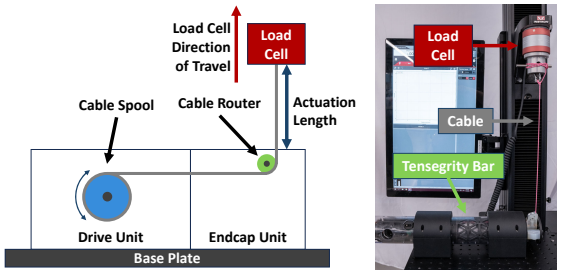

(a) (b)

Fig. 7. The (a) 2D diagram and (b) physical setup for cable length estimation and variable stiffness control testing. The cable is attached to the 5 kN load cell which is moved up and down. The actuation length is defined as the distance from the load cell to the tip of the pulley bracket.

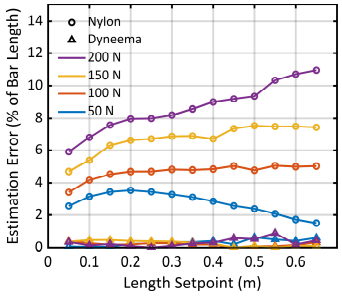

Fig. 8. Cable length estimation error scaled as a percentage of bar length (1.22 m) over a range of different cable lengths and cable forces.

B. Variable Stiffness Control

Variable stiffness control of the cable actuator was evaluated using the same experimental setup as the cable length accuracy test. The force response of the cable actuator was assessed by pulling the cable at a rate of 200 mm/s. A range of spring constants from 75 N/m to 280 N/m was tested, along with four different non-linear spring stiffness with varying exponential factors. For the linear stiffness, shown in Fig. 9a, the root mean squared error (RMSE) values were 3.75 N, 3.89 N, 3.28 N, 4.63 N for 75 N, 140 N, 210 N, and 280 N stiffness, respectively. For the non-linear stiffness, shown in Fig. 9b, the RMSE values were 2.81 N, 4.68 N, 5.66 N, and 4.73 N for $x^{8.0}$, $x^{5.5}$, $x^{0.55}$, $x^{0.45}$ stiffness curves, respectively. These results demonstrate that the cable actuator can be configured to behave as either a linear or non-linear spring. However, it should be noted that QDD actuators will have lower control bandwidth compared to systems with mechanical compliance.

IEEE Robotics and Automation Letters (RA-L) paper, presented at ICRA 2026, Vienna, Austria. Cite as RA-L paper.

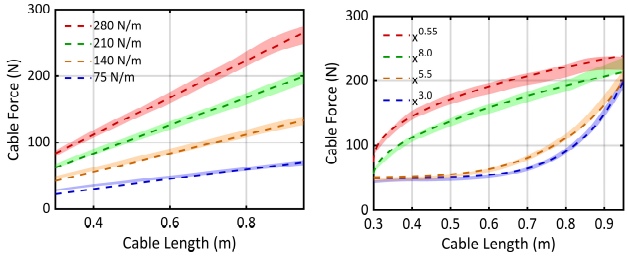

(a) (b)

Fig. 9. Variable stiffness control of cable force. (a) linear and (b) non-linear stiffness. The dashed lines represent the reference control curves while the measured force is represented by the shaded confidence interval.

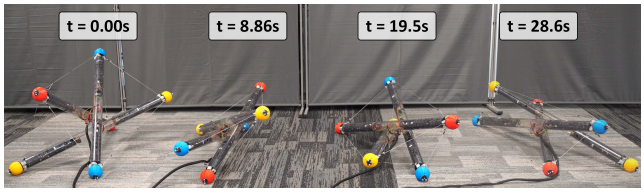

Fig. 10. Motion sequence of the tensegrity robot rolling forward, showing distinct positions over time.

C. Robot Testing

Robot locomotion was evaluated using teleoperation at 20 Hz, achieving 1.67 revolutions over 5.2 m in 28.6 s (0.15 BLPS), as shown in Fig. 10 and SI Video S1. This is faster than other meter-scale tensegrity robots such as Superballv1 [8] at 0.059 BLPS and Superballv2 [12] at 0.11 BLPS. Additional testing showed the robot capable of locomotion with a heavy (11 kg) payload. (SI Video S2).

On-the-fly stiffness tuning was tested by observing the robot shape, in particular the height, for varying stiffness and payload (SI Video S2). In Fig. 11a, the robot begins at 200 N/m cross cable stiffness with no payload, allowing it to achieve the target shape. Then, in Fig. 11b, a 9 kg payload is attached, causing the robot to sag under the added weight. The stiffness is subsequently increased to 450 N/m in Fig. 11c, enabling the robot to return to its target shape. Finally, in Fig. 11d the stiffness is lowered to 100 N/m, which is insufficient for carrying the payload and as a result, the robot to sags. The decoupling of shape and stiffness allows the robot to vary its compliance according to different situations and payload weights. Leveraging the shape morphing and variable stiffness tuning capabilities of the robot, height constrained navigation (Fig. 1b) and collapsed debris clearing (Fig. 1c) are demonstrated (SI Video S4, S5). These two experiments represent realistic scenarios in which the robot could navigate through an unstructured environment including height constrained obstacles.

Full robot state estimation was also tested during locomotion and the robot achieved a shape reconstruction RMSE of 3.2 PBL and average trajectory drift of 4.84% (final drift/trajectory length) [34]. Previous works in purely proprioceptive shape reconstruction have achieved at best 13.1 PBL RMSE [33]. Even with the use of external ranging [31] or camera [32] sensors, previous works have achieved at best 2.4 PBL RMSE. No previous tensegrity works have considered trajectory drift.

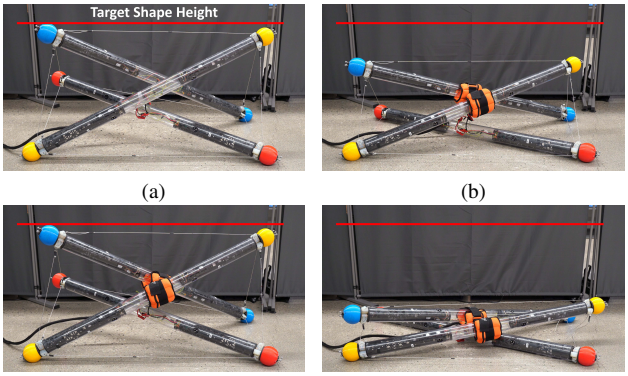

(a) (b) (c) (d)

Fig. 11. Variable stiffness control of the robot with constant target shape. The target shape's height is denoted by the horizontal red line. The robot starts at 200 N/m stiffness with (a) no payload, and (b) 9 kg payload (orange). The stiffness is then increased to (c) 450 N/m to return to starting shape, and then decreased to (d) 100 N/m.

TABLE II
COMPARISON WITH NASA SUPERBALL V2

Specification	This work	NASA SUPERballv2 [12]
Topology	3 Bar, Prism	6 Bar, Spherical
Actuated Cables	9	24
Cable Actuator	QDD	SEA
On-the-fly Stiffness Tuning	Yes	No
Bar Length	1.2 m	1.8 m
Min Locomotion Height	0.43 m	1.8 m
Locomotion Speed	0.15 BLPS	0.11 BLPS
Robot Weight	12 kg	38 kg
Max Payload	11 kg	-
Tethered	Yes	Yes

A full comparison between our work and most comparable tensegrity robot, NASA Superball, is presented in Tab. II. Notably, our three-bar design enables low-profile gaits for navigating height-constrained environments, supports heavy payloads, and incorporates the hardware necessary for full proprioceptive state estimation—an aspect not emphasized in Superball's design.

VII. CONCLUSION AND FUTURE WORKS

In this paper, we presented a novel design for a variable stiffness tensegrity robot utilizing QDD cable actuators. The QDD actuators significantly improve cable length estimation accuracy and enable on-the-fly stiffness tuning Experiments demonstrate <1 PBL cable length estimation error and force control of an arbitrary stiffness curve with <6 N of RMSE. The robot achieved rolling locomotion at 0.15 BLPS, exceeding the speeds of prior meter-scale tensegrity robots. It also demonstrated successful locomotion under a heavy (11 kg) payload, showcasing the robustness of the cable drive system. Accurate state estimation with 3.2 PBL RMSE in shape reconstruction and 4.84% average trajectory drift was achieved, surpassing previous proprioceptive methods and approaching the accuracy of external sensing-based approaches.

Future work will focus on incorporating additional computing and sensing modules, including cameras, to enable

untethered autonomous operation. The modular design enables optimization of sensor placement and an open-source standard for module design will enable collaborative, custom modules tailored to mission specific requirements. These developments lay the groundwork for enabling intelligent, autonomous tensegrity robots that can adapt to dynamic environments and payload conditions through enhanced sensing, locomotion optimization, and impact resistance.

ACKNOWLEDGMENT

The authors would like to acknowledge Eeshwar Krishnan for their help with robot fabrication.

REFERENCES

[1] R. E. Skelton and M. C. De Oliveira, *Tensegrity systems*. Springer, 2009, vol. 1.

[2] L.-H. Chen, B. Cera, E. L. Zhu, R. Edmunds, F. Rice, A. Bronars, E. Tang, S. R. Malekshahi, O. Romero, A. K. Agogino, and A. M. Agogino, "Inclined surface locomotion strategies for spherical tensegrity robots," in *2017 IEEE/RSJ International Conference on Intelligent Robots and Systems (IROS)*, 2017, pp. 4976–4981.

[3] C. Campos, R. Elvira, J. J. G. Rodríguez, J. M. Montiel, and J. D. Tardós, "ORB-SLAM3: An accurate open-source library for visual, visual–inertial, and multimap slam," vol. 37, no. 6, pp. 1874–1890, 2021.

[4] D. S. Shah, J. W. Booth, R. L. Baines, K. Wang, M. Vespignani, K. Bekris, and R. Kramer-Bottiglio, "Tensegrity Robotics," *Soft Robotics*, vol. 9, no. 4, pp. 639–656, Aug. 2022.

[5] J. M. Friesen, J. L. Dean, T. Bewley, and V. Sunspiral, "A Tensegrity-Inspired Compliant 3-DOF Compliant Joint," in *2018 IEEE International Conference on Robotics and Automation (ICRA)*. Brisbane, QLD: IEEE, May 2018, pp. 3301–3306.

[6] Q. Boehler, S. Abdelaziz, M. Vedrines, P. Poignet, and P. Renaud, "From modeling to control of a variable stiffness device based on a cable-driven tensegrity mechanism," *Mechanism and Machine Theory*, vol. 107, pp. 1–12, Jan. 2017.

[7] G. Pratt and M. Williamson, "Series elastic actuators," in *Proceedings 1995 IEEE/RSJ International Conference on Intelligent Robots and Systems. Human Robot Interaction and Cooperative Robots*, vol. 1. Pittsburgh, PA, USA: IEEE Comput. Soc. Press, 1995, pp. 399–406.

[8] A. P. Sabelhaus, J. Bruce, K. Caluwaerts, Y. Chen, D. Lu, Y. Liu, A. K. Agogino, V. SunSpiral, and A. M. Agogino, "Hardware design and testing of SUPERball, a modular tensegrity robot," in *2014 Edition of the World Conference on Structural Control and Monitoring (WCSCM)*, no. ARC-E-DAA-TN15339, 2014.

[9] B. M. Cera, A. A. Thompson, and A. M. Agogino, "Energy-Efficient Locomotion Strategies and Performance Benchmarks using Point Mass Tensegrity Dynamics," in *2019 IEEE/RSJ International Conference on Intelligent Robots and Systems (IROS)*. Macau, China: IEEE, Nov. 2019, pp. 4678–4683.

[10] L.-H. Chen, K. Kim, E. Tang, K. Li, R. House, E. L. Zhu, K. Fountain, A. M. Agogino, A. Agogino, V. Sunspiral, and E. Jung, "Soft Spherical Tensegrity Robot Design Using Rod-Centered Actuation and Control," *Journal of Mechanisms and Robotics*, vol. 9, no. 2, p. 025001, Apr. 2017.

[11] C. Paul, F. Valero-Cuevas, and H. Lipson, "Design and control of tensegrity robots for locomotion," *IEEE Trans. Robot.*, vol. 22, no. 5, pp. 944–957, Oct. 2006.

[12] M. Vespignani, J. M. Friesen, V. SunSpiral, and J. Bruce, "Design of SUPERball v2, a Compliant Tensegrity Robot for Absorbing Large Impacts," in *2018 IEEE/RSJ International Conference on Intelligent Robots and Systems (IROS)*. Madrid: IEEE, Oct. 2018, pp. 2865–2871.

[13] W. R. Johnson, A. Agrawala, X. Huang, J. Booth, and R. Kramer-Bottiglio, "Sensor Tendons for Soft Robot Shape Estimation," in *2022 IEEE Sensors*. Dallas, TX, USA: IEEE, Oct. 2022, pp. 1–4.

[14] K. Kim, A. K. Agogino, A. Toghyan, D. Moon, L. Taneja, and A. M. Agogino, "Robust learning of tensegrity robot control for locomotion through form-finding," in *2015 IEEE/RSJ International Conference on Intelligent Robots and Systems (IROS)*. Hamburg, Germany: IEEE, Sep. 2015, pp. 5824–5831.

[15] K. Kim, A. K. Agogino, D. Moon, L. Taneja, A. Toghyan, B. Dehghani, V. SunSpiral, and A. M. Agogino, "Rapid prototyping design and control of tensegrity soft robot for locomotion," in *2014 IEEE International Conference on Robotics and Biomimetics (ROBIO 2014)*. Bali, Indonesia: IEEE, Dec. 2014, pp. 7–14.

[16] S. Yagi, S. Kang, S. Yu, and H. Mahzoon, "Evaluation of Shape-Changing Tensegrity Structure Robot for Physical Human-Robot Interaction," in *2019 IEEE International Conference on Advanced Robotics and Its Social Impacts (ARSO)*. Beijing, China: IEEE, Oct. 2019, pp. 20–24.

[17] R. L. Baines, J. W. Booth, and R. Kramer-Bottiglio, "Rolling Soft Membrane-Driven Tensegrity Robots," *IEEE Robot. Autom. Lett.*, vol. 5, no. 4, pp. 6567–6574, Oct. 2020.

[18] M. Khazanov, B. Humphreys, W. Keat, and J. Rieffel, "Exploiting Dynamical Complexity in a Physical Tensegrity Robot to Achieve Locomotion," in *Advances in Artificial Life, ECAL 2013*. MIT Press, Sep. 2013, pp. 965–972.

[19] X. Xu, T. Zhang, S. Wang, X. Li, Y. Chen, Y. Li, B. Raj, M. Johnson-Roberson, and X. Huang, "From Perfect to Noisy World Simulation: Customizable Embodied Multi-modal Perturbations for SLAM Robustness Benchmarking," 2024.

[20] Z. Li, P. Xu, and B. Li, "A novel variable stiffness actuator based on cable-pulley-driven mechanisms for robotics," *IEEE/ASME Transactions on Mechatronics*, pp. 1–12, 2024.

[21] P. M. Wensing, A. Wang, S. Seok, D. Otten, J. Lang, and S. Kim, "Proprioceptive Actuator Design in the MIT Cheetah: Impact Mitigation and High-Bandwidth Physical Interaction for Dynamic Legged Robots," *IEEE Trans. Robot.*, vol. 33, no. 3, pp. 509–522, Jun. 2017.

[22] R. E. Skelton, J. W. Helton, R. Adhikari, J.-P. Pinaud, and W. Chan, "An introduction to the mechanics of tensegrity structures," in *The mechanical systems design handbook*. CRC Press, 2017, pp. 315–388.

[23] S. Seok, A. Wang, D. Otten, and S. Kim, "Actuator design for high force proprioceptive control in fast legged locomotion," in *2012 IEEE/RSJ International Conference on Intelligent Robots and Systems*. Vilamoura-Algarve, Portugal: IEEE, Oct. 2012, pp. 1970–1975.

[24] R. Goyal, M. Chen, M. Majji, and R. Skelton, "Motes: Modeling of tensegrity structures," *Journal of Open Source Software*, vol. 4, p. 1613, 10 2019.

[25] D. Gueners, H. Chanal, and B.-C. Bouzgarrou, "Design and implementation of a cable-driven parallel robot for additive manufacturing applications," *Mechatronics*, vol. 86, p. 102874, Oct. 2022.

[26] J. Bruce, K. Caluwaerts, A. Iscen, A. P. Sabelhaus, and V. SunSpiral, "Design and evolution of a modular tensegrity robot platform," in *2014 IEEE International Conference on Robotics and Automation (ICRA)*. Hong Kong, China: IEEE, May 2014, pp. 3483–3489.

[27] H. A. McKenna, J. W. S. Hearle, and N. O'Hear, *Handbook of fibre rope technology*. Woodhead publishing, 2004, vol. 34.

[28] A. Pott and T. Bruckmann, *Cable-driven parallel robots*. Springer, 2013.

[29] D. Gueners, B.-C. Bouzgarrou, and H. Chanal, "Cable Behavior Influence on Cable-Driven Parallel Robots Vibrations: Experimental Characterization and Simulation," *Journal of Mechanisms and Robotics*, vol. 13, no. 4, p. 041003, Aug. 2021.

[30] A. S. Huang, E. Olson, and D. C. Moore, "LCM: Lightweight Communications and Marshalling," in *2010 IEEE/RSJ International Conference on Intelligent Robots and Systems*. Taipei: IEEE, Oct. 2010, pp. 4057–4062.

[31] K. Caluwaerts, J. Bruce, J. M. Friesen, and V. SunSpiral, "State estimation for tensegrity robots," in *2016 IEEE International Conference on Robotics and Automation (ICRA)*. Stockholm, Sweden: IEEE, May 2016, pp. 1860–1865.

[32] S. Lu, W. R. J. I. au2, K. Wang, X. Huang, J. Booth, R. Kramer-Bottiglio, and K. Bekris, "6n-dof pose tracking for tensegrity robots," in *Robotics Research*, A. Billard, T. Asfour, and O. Khatib, Eds. Cham: Springer Nature Switzerland, 2023, pp. 136–152.

[33] J. W. Booth, O. Cyr-Choinière, J. C. Case, D. Shah, M. C. Yuen, and R. Kramer-Bottiglio, "Surface Actuation and Sensing of a Tensegrity Structure Using Robotic Skins," *Soft Robotics*, vol. 8, no. 5, pp. 531–541, Oct. 2021.

[34] W. Tong, T.-Y. Lin, J. Mi, Y. Jiang, M. Ghaffari, and X. Huang, "Tensegrity robot proprioceptive state estimation with geometric constraints," *IEEE Robotics and Automation Letters*, vol. 10, no. 4, pp. 4069–4076, 2025.